JOURNAL OF SPACECRAFT AND ROCKETS
Vol. 35, No. 5, September–October 1998

Unsteady Effects of Dissociative Cooling Under High-Stagnation-Point Heat Loads

Benjamin P. Lacy,* Philip L. Varghese,† and Dennis E. Wilson‡
University of Texas at Austin, Austin, Texas 78712-1085

By embedding a solid dissociating material into the porous outer structure of a projectile subjected to high-stagnation-point heating, internal cooling may be achieved from the dissociation of the heated material and by the subsequent outgassing of the products. Ammonium chloride, NH_4Cl, which absorbs substantial energy upon dissociation into ammonia and hydrogen chloride at temperatures over 613 K, is the principal material considered. Stagnation-point heat transfer solutions for the injection of the dissociation products of NH_4Cl have been developed and are coupled to a model of the internal heat and mass transfer through the porous medium to calculate the transient temperature profiles during the flight of the body. Results show that dissociative cooling has the potential to slow the rate of temperature rise of the body.

Nomenclature

c_i = mass fraction of species i
c_p = specific heat per unit mass at constant pressure, J/kg · K
$\bar{c}_p$ = mass average specific heat of gas mixture, J/kg · K
D = binary diffusion coefficient, m^2/s
h = enthalpy, J/kg
j = diffusive mass flux, kg/m^2 · s
K = permeability, m^2
k = thermal conductivity, W/m · K
M = molar mass
$\dot{M}$ = blowing parameter, $\rho_w v_w / \sqrt{\rho_e \mu_e \kappa}$
$\dot{m}$ = mass flow rate, kg/m^2 · s
$\dot{N}$ = molar flux, mol/s · m^2
Nu = Nusselt number, $q_w x/(T_e - T_w)k$
P = pressure, N/m^2
q = heat flux, W/m^2
R = gas constant
Re = Reynold's number, $u_e x/v$
T = temperature, K
U = diffusion velocity, m/s
y = distance normal to body surface (into the body), m
δ = incremental spacing, m
θ = T/T_e
κ = velocity gradient, $\partial u_e/\partial x$, at the stagnation point
μ = viscosity, kg/s · m
ν = kinematic viscosity, m^2/s
ρ = density, kg/m^3
v = one-dimensional velocity in the porous media, m/s
Φ = viscous dissipation
ϕ = porosity
χ_i = mode fraction of species i

Subscripts and Superscripts

amb = ambient
diss = dissociation
e = boundary-layer edge
eff = effective
f = formation
i = ith species
int = interface of dissociating material
m = gas mixture
N = total number of species
S = solid
vol = averaged over entire volume
w = wall

Received Aug. 19, 1997; revision received Dec. 25, 1997; accepted for publication April 8, 1998.

*Research Assistant, Institute for Advanced Technology; currently Engineering Associate, Process Development, Cabot Corp., Pampa, TX 79065. Member AIAA.
†Professor, Department of Aerospace Engineering and Engineering Mechanics. Senior Member AIAA.
‡Associate Professor, Institute for Advanced Technology. Member AIAA.

Introduction

PROJECTILES, traveling at hypervelocity, experience huge heat fluxes that result in ablation of the outer skin. The ablated material absorbs and carries away energy and provides a boundary layer to reduce heat transfer to the body. However, this loss of material alters the body's shape and the flow characteristics. This paper continues an investigation of an alternative means of providing cooling called dissociative cooling.[1,2]

Dissociative cooling involves the embedding of a dissociating material into the porous outer structure of a projectile (see Fig. 1). The principal material considered here is ammonium chloride, NH_4Cl. At 1 atm, NH_4Cl begins to dissociate into ammonia and hydrogen chloride at 613 K (Ref. 3) and has a high enthalpy of dissociation, approximately 3100 kJ/kg (Ref. 4). As the dissociation products flow through the porous structure to the hotter outer surface, the gas temperature will increase further, and the ammonia could break down into nitrogen and hydrogen. The dissociations and gas flow will absorb energy that would otherwise have gone to heating the projectile. The outflowing gas mixture will provide transpiration cooling, reducing the heat transfer to the surface. This effect was first examined in Ref. 1, which examined the heat transfer reduction for injection of NH_4Cl into both equilibrium and frozen boundary layers. These results were presented for various blowing rates and also compared with more traditional transpiration studies that used air and helium as injection gases. Reference 2 summarizes some of the experimental results of this investigation, demonstrating that the rise in temperature through porous beds doped with NH_4Cl is less than for undoped beds or beds doped with a control material ($MgSO_4$) that has similar thermal properties but does not dissociate. That paper also demonstrated that the transient temperature profiles inside the porous medium can be modeled if the mass distribution, dissociation rate, and effective thermal conductivity of the bed are known accurately.

Other materials, such as aluminum nitride and boron nitride, have even greater enthalpies of dissociation but dissociate at much higher temperatures. Ammonium chloride begins dissociation at 613 K at 1 atm. At 100 atm (from Antoine's equation), the dissociation begins at 869 K (Ref. 3). This temperature range is low enough to provide thermal protection when needed but not so low that all of the ammonium chloride will have dissociated before the projectile's flight is completed.

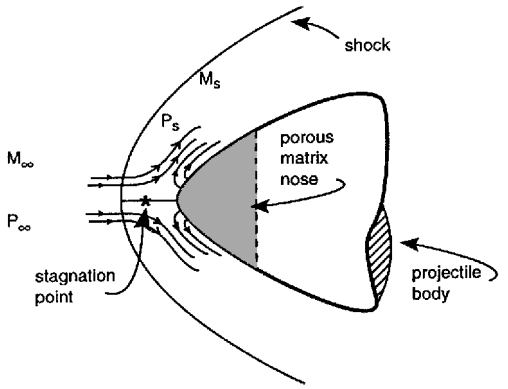

Fig. 1 Dissociative cooling concept.

The present paper will utilize the results of Ref. 1, where the stagnation-point heat transfer rate reduction due to NH_4Cl dissociation was computed. This solution is a multispecies version similar to previous studies that used similarity analysis to determine the effects on heat transfer of air injection at the stagnation point.[5,6] Those results will provide the surface boundary conditions needed to determine the time-dependent temperature profile in a porous body doped with NH_4Cl. This will allow an examination of the overall effectiveness of dissociative cooling in extending the potential flight time of a projectile or other body.

Mathematical Model

Surface Boundary Conditions

Reference 1 solved the exterior flow equations around the stagnation point for the injection of the products of NH_4Cl under a variety of wall and boundary-layer conditions. The solutions provided the heat transfer rate and species concentration at the wall as a function of mass injection rate (dissociation rate of NH_4Cl). The heat transfer rate can be expressed nondimensionally as

$$\frac{Nu}{\sqrt{Re_e}} = \frac{|q_w|\sqrt{\nu_e/\kappa}}{(T_e - T_w)k_e} \tag{1}$$

Figure 2 shows the heat transfer rate as a function of the injection parameter $\dot{M}$ for a blunt-body projectile traveling at Mach 10 at an altitude of 54.9 km for $\theta_w = 0.25$ and 0.5, assuming a completely frozen boundary layer with noncatalytic wall. As can be seen, for this case the variation in $Nu/\sqrt{Re_e}$ is principally dependent on the variation in mass injection, not the wall temperature ratio. Similar results are obtained for the concentration of the various species at the wall.

The independence of $Nu/\sqrt{Re}$ from the wall temperature ratio allows for a decoupling of the interior and exterior flow solutions, so that the surface conditions can be determined solely by the projectile flight conditions and the mass injection parameter

$$\dot{M} = \frac{\rho_w \upsilon_w}{\sqrt{\rho_e \mu_e \kappa}} \tag{2}$$

at the surface at a given time during the flight (where we assume that the solution at one time has no effect on the solution at a later time).

Reference 1 also showed the process to be most effective for bodies of large radius, at high altitudes, because for a given injection rate (dissociation rate) the mass injection parameter is inversely proportional to radius and ρ_e. The dissociation rate was estimated using an empirical extrapolation of experimental results giving the forward reaction rate of NH_4Cl vs temperature[7]

$$\dot{N}(\text{mol/s m}^2) = \phi 9689 e^{-6126.4/T_{\text{int}}} \tag{3}$$

Even at high temperatures, the recession rate given by

$$\dot{y}_{\text{int}} = \frac{\dot{m}_{\text{diss}}}{\rho_{\text{vol, NH4CL}}} \tag{4}$$

is found to be small for sufficiently large radius bodies, where the process is reasonably effective in reducing heat transfer. All of the

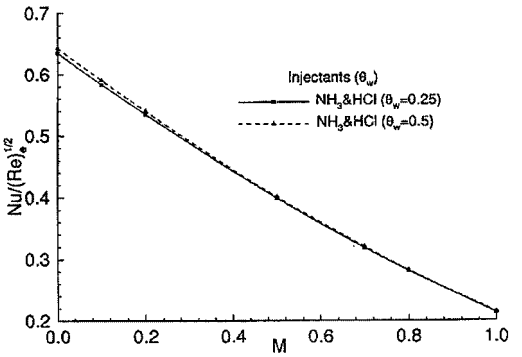

Fig. 2 Effect of temperature ratio on heat transfer in frozen boundary layer with noncatalytic wall.

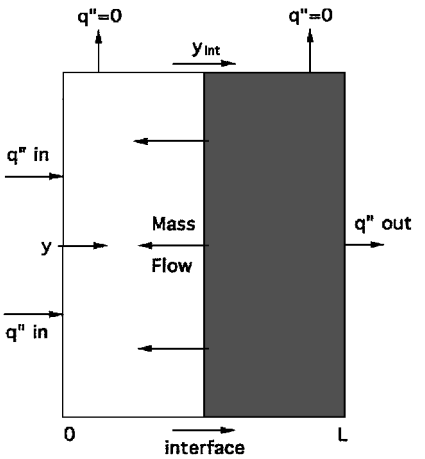

Fig. 3 One-dimensional model of porous medium with dissociating NH_4Cl.

flow is therefore assumed outward through the surface. Also, dissociation will be greatest at the nose, which is the point of highest heat transfer. The gas outflow will be prevented from moving laterally because the sides will still contain the dissociating material. However, to ensure outflow to the stagnation point, it may be necessary to design the porous matrix to preferentially direct the flow toward the surface. The recession rate assumes that the interface is along one surface in the body, with no NH_4Cl beneath the interface dissociating before all of the NH_4Cl at or above the interface dissociates.

Flow Through the Porous Medium

The first step in developing a solution is the formulation of the equations for the flow through the porous medium. Because the recession rate, relative to projectile radius, was shown to be small for most cases, we use a one-dimensional transient model (Fig. 3). The model is a semi-infinite porous plane with stagnation-point heat transfer occurring at one side and a moving interface of ammonium chloride within. All heat transfer and mass flow is assumed to be in the y direction. For a known dissociation rate, at the NH_4Cl interface, the time-dependent flow through the porous medium can be determined.

The continuity equation for flow through the porous medium is

$$-\frac{\partial \dot{m}}{\partial y} = \phi \frac{\partial \rho}{\partial t} \tag{5}$$

The flow rate can be determined from Darcy's law,[8]

$$\bar{\upsilon} = -\frac{K}{\mu}\frac{\partial P}{\partial y} \tag{6}$$

which provides a relationship between the flow velocity, pressure gradient, and material permeability. Thus, the mass flow rate is given by

$$\dot{m} = \rho \bar{\upsilon} = -K\frac{\rho}{\mu}\frac{\partial P}{\partial y} \tag{7}$$

Assuming an ideal gas, the equation of state is given by

$$P = \rho RT \tag{8}$$

Using these three equations, we obtain the combined equation of flow

$$\frac{\partial}{\partial y}\left[\frac{K}{\mu}R\rho\frac{\partial}{\partial y}(\rho T)\right] = \phi\frac{\partial\rho}{\partial t} \tag{9}$$

At the surface ($y = 0$), the density at the stagnation point is determined from the given flight conditions. At the interface of the ammonium chloride ($y = y_{\text{int}}$), the mass flow computed from Darcy's law is set equal to the dissociation rate determined earlier as a function of temperature. These boundary conditions can be written as

$$\rho\,(y = 0) = \rho_w \tag{10}$$

$$-\frac{K}{\mu}R\rho\frac{\partial}{\partial y}(\rho T)_{y_{\text{int}}} = \dot{m}_{\text{diss}} \tag{11}$$

The initial conditions are $\dot{m}\ (t = 0) = 0$, except at the ammonium chloride interface, $T\ (t = 0) = T_{\text{initial}}$, and $\rho\ (t = 0) = \rho_w$.

To estimate the timescales for thermal and flow equilibration, an idealized model is first solved. The combined equations of flow are solved using finite difference methods. Figures 4 and 5 show the mass flow rate as a function of position at several times in a porous medium at a constant uniform temperature of 1000 K. The mass flow rate at the interface undergoes a step increase from 0 to $\dot{m}_{\text{diss}}\ (T_{\text{int}})$ at $t = 0$, and the gas phase is assumed to be NH_3 and HCl in equal proportions with a stationary interface at $y = 1$ m. Figures 4 and 5 show different permeabilities. For a medium with reasonably high permeability and low thermal conductivity, $\dot{m}$ goes to $\dot{m}_{\text{diss}}$ on a very short timescale (order of seconds) compared with the thermal penetration time[9] defined by

$$t = \frac{\rho c_p L^2 \phi}{12 k_{\text{eff}}} \tag{12}$$

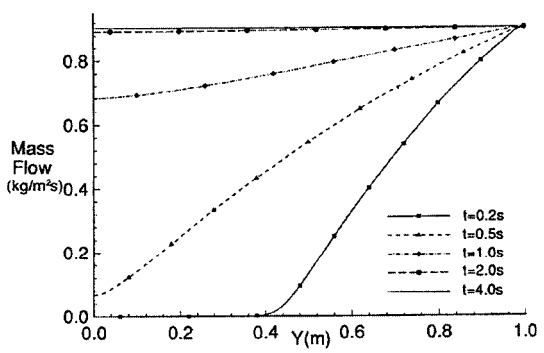

Fig. 4 Mass flow rate in a porous medium undergoing a step increase in flow on one side with $K = 10^{-11}$ m^2 and $\phi = 0.8$.

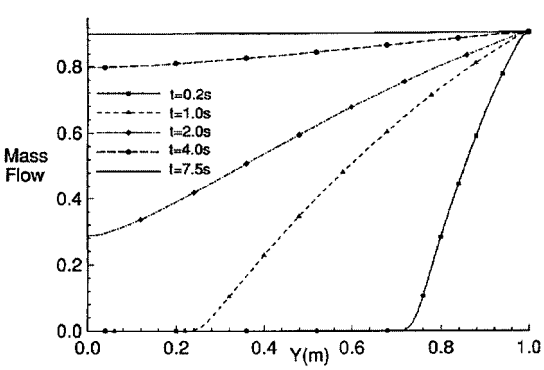

Fig. 5 Mass flow rate in a porous medium undergoing a step increase in flow on one side with $K = 10^{-12}$ m^2 and $\phi = 0.8$.

This time determines the rate at which temperature changes propagate through the medium. For Al_2O_3 with $\phi = 0$, the penetration time is about 14 h. Hence the mass flow rate can be assumed to be in equilibrium throughout the porous medium.

This allows a substantial simplification when solving the internal flow problem because the flow rate through the medium does not have to be solved continuously. Instead, the flow rate at any point in the body will be equal to the instantaneous/current dissociation rate. As the dissociation rate changes, and the interface moves, only the pressure field in the medium need be computed. This can be done using Darcy's law in the form

$$\dot{m}_{\text{diss}} = -\frac{K}{\mu}\frac{P}{RT}\frac{\partial P}{\partial y} \tag{13}$$

which can be solved through the medium to the interface from the known pressure at the surface. The $\dot{m}_{\text{diss}}$ is determined using Eq. (3).

Energy Equation

Having evaluated the effects of bulk flow through a porous medium, the specific problem of heat-up of a porous medium embedded with a dissociating material is now addressed. The energy equations in enthalpy form must be solved to obtain the temperature profile through the porous medium as a function of time. Downstream of the dissociating interface, the equation for the gas mixture is[10]

$$\rho m\frac{\partial h_m}{\partial t} + (\rho\upsilon)_m\frac{\partial h_m}{\partial y} - \upsilon\frac{\partial P}{\partial y} - \frac{\partial P}{\partial t} = \frac{\partial}{\partial y}\left(k_{\text{eff}}\frac{\partial T}{\partial y} - \sum_i^N \rho_i U_i h_i\right) + \mu\Phi \tag{14}$$

and for the porous solid it is

$$\rho_s\frac{\partial h_s}{\partial t} = \frac{\partial}{\partial y}k_{\text{eff}}\frac{\partial T}{\partial y} \tag{15}$$

where there are N gas products plus the porous solid. These equations are based on the following assumptions:

1) The flow is approximately one dimensional.

2) The temperature at each point is the same for both the gas and the porous medium (one-temperature approximation).

3) The thermal conductivity k_{eff} can be reasonably estimated.

4) Radiation heat transfer is neglected.

Integrating over the pore area, one can show[11] that

$$\mu\int\Phi\,\mathrm{d}A = -\upsilon A\frac{\partial P}{\partial y} \tag{16}$$

The one-temperature approximation and Eq. (16) for $\mu\Phi$ are combined to give

$$(1-\phi)\rho_s\frac{\partial h_s}{\partial t} + \phi\rho_m\frac{\partial h_m}{\partial t} + \dot{m}\frac{\partial h_m}{\partial y} - \phi\frac{\partial P}{\partial t} = \frac{\partial}{\partial y}\left(k_{\text{eff}}\frac{\partial T}{\partial y} - \sum_i^N \rho_i U_i h_i\phi\right) \tag{17}$$

where $\dot{m} = -\dot{m}_{\text{diss}}$. This equation can be converted to temperature using

$$\frac{\partial h_m}{\partial y} = \bar{c}_p\frac{\partial T}{\partial y} + \sum_i h_i\frac{\partial c_i}{\partial y} \tag{18}$$

$$\frac{\partial h_m}{\partial t} = \bar{c}_p\frac{\partial T}{\partial t} + \sum_i h_i\frac{\partial c_i}{\partial t} \tag{19}$$

and species continuity

$$\rho\frac{\partial c_i}{\partial t} + \rho\upsilon\frac{\partial c_i}{\partial y} = -\frac{\partial\rho_i U_i}{\partial y} \tag{20}$$

to obtain the equation that applies downstream of the interface:

$$[\rho_s c(1-\phi)+\rho_m \bar{c}_p \phi]\frac{\partial T}{\partial t}+\dot{m}\bar{c}_p\frac{\partial T}{\partial y}-\phi\frac{\partial P}{\partial t}$$
$$=\frac{\partial}{\partial y}k_{\text{eff}}\frac{\partial T}{\partial y}-\sum_i \rho_i U_i \phi\frac{\partial T}{\partial y}c_{pi} \tag{21}$$

Upstream of the interface, the energy equation is the solid body transient conduction equation

$$[\rho_s c(1-\phi)+\phi(\rho c_p)_{\text{NH}_4\text{Cl}}]\frac{\partial T}{\partial t}=\frac{\partial}{\partial y}k_{\text{eff}}\frac{\partial T}{\partial y} \tag{22}$$

This assumes a porous medium that is fully packed with NH_4Cl in the matrix interstitial sites. The k_{eff} for the different regions depends on the porosity, the materials involved, and how they are arranged in the matrix.

The boundary conditions at the surface are

$$q_w=-k\left(\frac{\partial T}{\partial y}\right)_w \tag{23}$$

$$\chi_{iw}=\chi_{i(y=0)} \tag{24}$$

At the interface, an energy balance yields

$$(\rho c_p)_{\text{vol}}\frac{\partial T}{\partial t}+\bar{c}_p\frac{\partial \dot{m}T}{\partial y}-\bar{c}_p T\frac{\partial \dot{m}}{\partial y}-\phi\frac{\partial P}{\partial t}$$
$$=-\sum_i \phi\frac{\partial \rho_i U_i T}{\partial y}c_{pi}+\sum_i T\phi\frac{\partial \rho_i U_i}{\partial y}c_{pi}$$
$$+\frac{\partial}{\partial y}k_{\text{eff}}\frac{\partial T}{\partial y}+\frac{\dot{m}_{\text{diss}}h_f}{\delta} \tag{25}$$

All dissociation is assumed to occur at the interface with no recombination in the gas flow. At $y=\infty$,

$$T(\infty)=T_{\text{amb}} \tag{26}$$

The initial conditions are $T=T_{\text{amb}}$, $\chi_{\text{air}}=1.0$, and $y_{\text{int}}=0.0$. The recession rate is then calculated and the interface location tracked with time.

Gas Mixture Concentrations

The wall boundary conditions are determined from the solution to the outer flow problem as described in Ref. 1. The heat transfer and wall concentrations can be found from the known wall temperatures at the selected flight conditions. The gas concentrations of different species at a given time and the diffusional velocities of those species through the medium are also needed to solve the energy equation. Knowing the surface concentrations at a given time and the mass flow rate from the dissociation rate equation, these quantities can be obtained using the Stefan–Maxwell equation[12]

$$\frac{\partial \chi_i}{\partial y}=\sum_j \frac{M_m}{\rho D_{ij}}(\chi_i \dot{N}_j-\chi_j \dot{N}_i) \tag{27}$$

This equation can be solved iteratively to find the concentration profiles from the surface to the interface. Using the concentration and pressure profiles, one can find M_m, ρ_m, and the species velocity

$$\upsilon_i=\frac{M_m}{M_{\text{NH}_4\text{Cl}}}\frac{\dot{m}_{\text{diss}}}{\rho_m \chi_i} \tag{28}$$

for the NH_4Cl products. Assuming no net air inflow, $\upsilon_i=0$ for the air products. (Recession rate will be slow relative to gas velocity out.) The diffusional velocity is

$$U_i=\upsilon_i-\upsilon_m \tag{29}$$

At a given time step, the Stefan–Maxwell equation must be solved concurrently with Darcy's law in the form given by Eq. (13).

Numerical Solution and Results

The compressible boundary-layer equations were transformed to boundary value problems and solved using shooting with Newton iteration. A fourth-order Runge–Kutta integrator was used to solve the mass, species, momentum, and energy equations. A minimum of 500 points was used on all equations, and the iteration was continued until the wall boundary conditions were satisfied using a relative error tolerance of 10^{-5}. Reference 1 contains further details of the numerical solution procedure.

The solution of the energy equation, Darcy's law, and the Stefan–Maxwell equation were solved through the porous media using finite differencing. Darcy's law and the Stefan–Maxwell equation were solved simultaneously using forward differencing for a truncation accuracy on the order of Δx.

At each time step, the solution of these equations was used in solving the energy equation for that time step. The energy equation was solved using forward time, centered space differencing for truncation errors on the order of Δt and Δx^2. A $\Delta x/L$ of less than 0.0001 was used to minimize truncation error. Both time and spatial step size were successively varied until the results were independent of their size. Stability was ensured by selecting a sufficiently small time step relative to Δx.

Both the external boundary-layer heat transfer problem and the internal equations modeling the flow through the porous media were solved on a SPARC Station IPC.

Numerical simulations were conducted to assess the relative effect of porosity, permeability, and nose radius on the temperature profiles at various times. In all cases, the aerothermodynamic environment was constant, as defined by a Mach 10 flight at 54.9-km altitude with a frozen boundary layer and noncatalytic wall assumption. Figures 6–9 show data for a low-porosity ($\phi=0.2$) matrix, and Figs. 10–13 show data for a high-porosity ($\phi=0.8$) matrix. The effects of first varying permeability and the nose radius are investigated to determine the overall effectiveness in reducing the temperature. The last result, given by Fig. 14, shows the effect of a two-layer model for permeability.

Figure 6 shows the temperature profiles for a body of radius 0.1 m with a fully packed porosity of 0.2. The porous matrix has ρc equal to that of aluminum oxide ceramic. An effective thermal conductivity of $k_{\text{eff}}=0.1$ W/mK was used throughout the body. Low thermal conductivities were used throughout this section because the higher

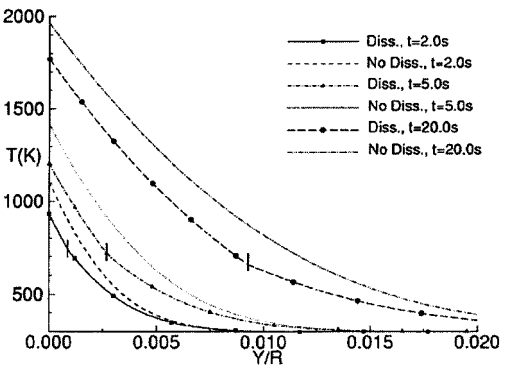

Fig. 6 Temperature profiles at various times for a large (0.1-m) nose radius body with k_{eff} = 0.1 W/mK and ϕ = 0.2.

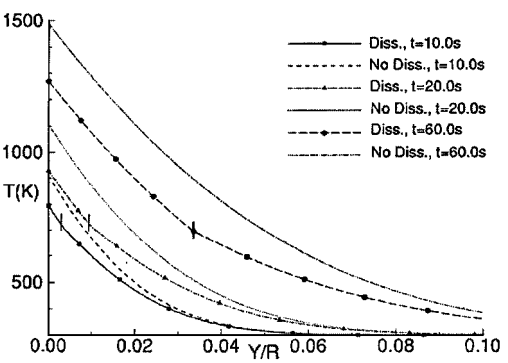

Fig. 7 Temperature profiles at various times for a large (0.1-m) nose radius body with k_{eff} = 1.0 W/mK and ϕ = 0.2.

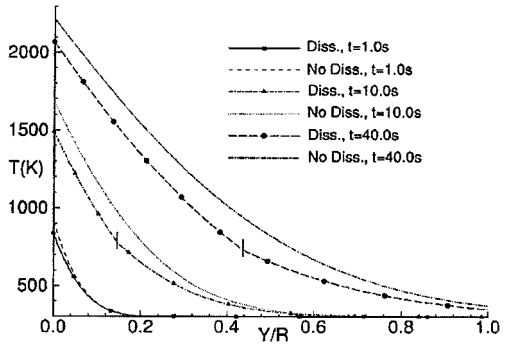

Fig. 8 Temperature profiles at various times for a small (0.01-m) nose radius body with k_{eff} = 1.0 W/mK and ϕ = 0.2.

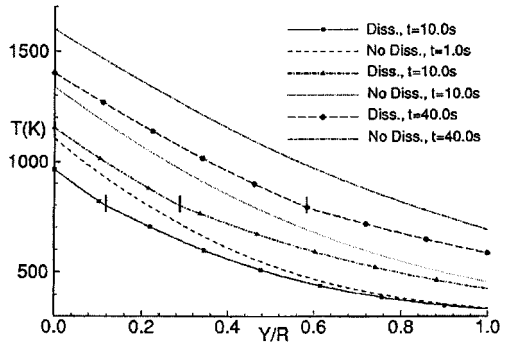

Fig. 9 Temperature profiles at various times for a small (0.01-m) nose radius body with k_{eff} = 5.0 W/mK and ϕ = 0.2.

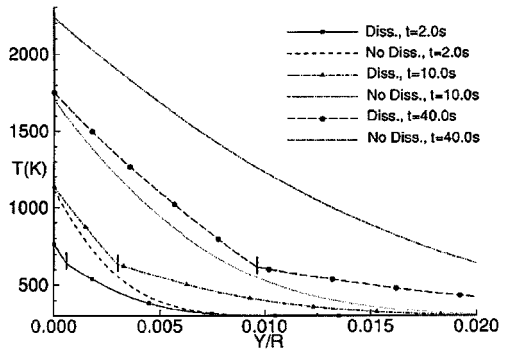

Fig. 10 Temperature profiles at various times for a large (0.1-m) nose radius body with k_{eff} = 0.1 W/mK and ϕ = 0.8.

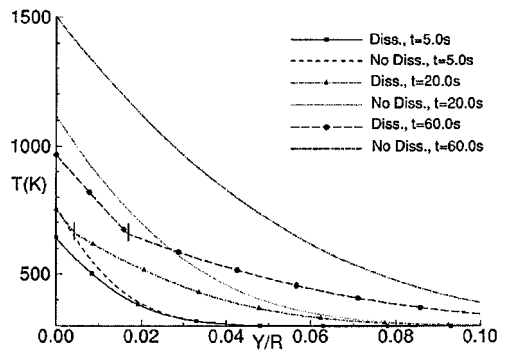

Fig. 11 Temperature profiles at various times for a large (0.1-m) nose radius body with k_{eff} = 1.0 W/mK and ϕ = 0.8.

the thermal conductivity, the longer it took to obtain sufficient temperature rise and, hence, the longer the computer run time. As will be seen, the magnitude of the thermal conductivity is much less significant than the differences in thermal conductivity through the body. Figure 6 shows that temperatures for the case where dissociation and subsequent transpiration occurs are significantly lower than for the case without dissociation. At 20 s into the flight, the surface temperature difference has peaked and started to decrease

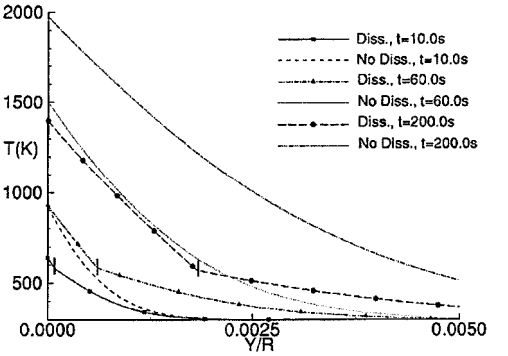

Fig. 12 Temperature profiles at various times for a very large (1.0-m) nose radius body with k_{eff} = 0.1 W/mK and ϕ = 0.8.

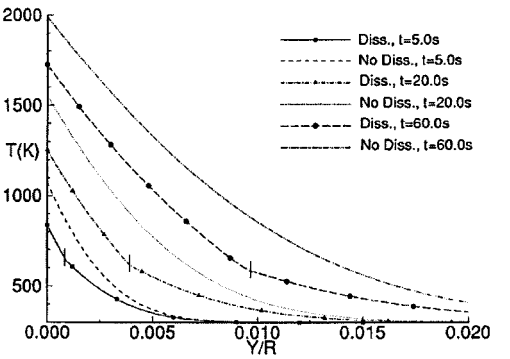

Fig. 13 Effect of artificially increasing ρc on the temperature profiles at various times for a large (0.1-m) nose radius body with k_{eff} = 0.1 W/mK and ϕ = 0.8.

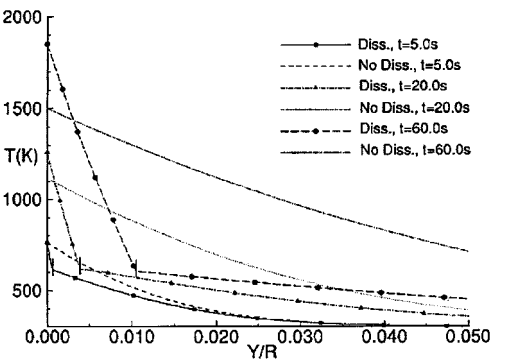

Fig. 14 Effect of discontinuous permeability, k_{eff} = 0.1 W/mK downstream and k_{eff} = 1.0 W/mK upstream, on the temperature profiles for a large (0.1-m) nose radius body with ϕ = 0.8.

slightly as the interface recedes. At this time, the interface, identified by the discontinuity in the slope of the line, has receded about 1% of the body radius into the body. The interface temperature initially increases rapidly and then levels off and remains relatively constant, decreasing slightly as it recedes deeper into the body.

Figure 7 is for the same body but with k_{eff} = 1.0 W/mK. As can be seen, the temperature rise is much slower, but the maximum temperature difference is about the same, though it occurs at later times and with the interface farther away from the surface due to the swifter conduction of heat into the body. The interface temperature is about the same.

Figure 8 illustrates a body with the same thermal properties and geometry as Fig. 7 but with a radius of 0.01 m. This corresponds to a higher heat transfer rate and hence a more rapid temperature rise. Because the heat transfer rate is greater, the interface temperature is higher, and therefore the interface recession is faster. The temperature differences are not quite as great but are still fairly large, even after the interface has receded significantly. The one-dimensional approximation is probably not adequate for a body this small, as the recession distance is significant compared with the radius. Figure 9 is for the same body but with k_{eff} = 5.0 W/mK.

As expected, the temperature rise is slower, but the magnitude of the difference is about the same. The interface temperature is also about the same as in Fig. 8.

Figure 10 shows results for a body with a radius of 0.1 m and $k_{\text{eff}} = 0.1$ W/mK but with a fully packed porosity of 0.8, which gives a higher dissociation rate for a given interface temperature. The temperature differences are much greater than those in Fig. 6, the interface temperatures are lower, and hence the recession rate is slower. Thus, the time the body will be protected is greater. Figure 11 is for the same body but with $k_{\text{eff}} = 1.0$ W/mK. The maximum temperature difference is about the same as the difference shown in Fig. 10. The principal change is the time lag before the temperature rise, similar to what was seen when varying k_{eff} for a body with $\phi = 0.2$.

Figure 12 is for a body with the same thermal properties and geometry as Fig. 10 but with a radius of 1.0 m. Because the heat transfer is reduced and the transpiration cooling part of the process is more effective as discussed earlier, the interface temperature is lower and the recession rate slower. The temperature differences are very substantial even at long times.

Figure 13 is for a body with the same thermal properties and geometry as Fig. 10 but with a heat capacity 10 times as large. Because of the large heat capacity, the temperature rise is slower, and interface temperature is slightly lower. Temperature differences are reduced, though they are still significant, particularly considering the magnitude of the increase in heat capacity and the consequent reduction in the rate of temperature rise.

Figure 14 is for the same body as Fig. 10 but with $k_{\text{eff}} = 0.1$ W/mK downstream of the interface and 1.0 W/mK upstream of the interface. As the interface moves away from the surface, the temperature downstream of the interface rises rapidly above that for the case without dissociation. Obviously the much higher thermal conductivity outweighs the effects of dissociation in carrying away heat. It therefore follows that dissociative cooling may not be effective if there is a substantial change in thermal conductivity across the interface. One may conclude that, if the thermal conductivity of the solid is decreased significantly by making it into a porous matrix, the process may not be as effective as using a solid projectile tip.

The other major unknown in all of these calculations was the permeability K. However, the variation of K has almost no effect on the temporal results. Substantial changes in flow density and pressure in the body have little effect on the energy equation, even at porosities approaching unity. The temperature gradient effects outweigh these effects by a large margin. However, pressure and density changes do have an effect (not considered here) because they can alter the dissociation rate from the empirical relation used in these calculations, and they also affect any subsequent dissociation/recombination within the flowstream.

Although the effect on the heat transfer to the surface by the outgassing of the dissociated NH_4Cl can be compared with the standard works,[5,6] there are no data on the composite effect of breakdown and outgassing of a dissociating material in a porous medium to compare with the results presented here. An experimental test will be required to confirm these results.

Conclusions

It has been shown that dissociative cooling can provide a significant reduction in the rate of temperature rise of a body subjected to high-stagnation-point heat loads. This thermal protection is achieved through a combination of internal cooling from the NH_4Cl dissociation and a reduction in heat transfer to the body from transpiration cooling.

Results of modeling a projectile traveling at Mach 10 at 54.9 km with a frozen boundary layer and noncatalytic wall show the scenarios for which the dissociative cooling process is most effective. For a projectile of $\phi = 0.2$ and $r = 0.1$ m made of Al_2O_3, the surface temperature is about 16% less 2 s into the flight and still 8% less 20 s into the flight. If porosity is increased to $\phi = 0.8$, the surface temperature is reduced about 30% at 2 s and 20% at 40 s. If the radius is increased to 1.0 m with $\phi = 0.8$, the surface temperature is reduced 30% at 10 s, about 39% at 60 s, and 30% at 200 s. The process can be seen to be most effective for large-radius bodies with high porosity, i.e., more NH_4Cl.

The thermal conductivity of the material to be protected is also important. If the thermal conductivity of a solid is decreased substantially when formed into a porous matrix, then dissociative cooling may not be effective. Also, if the effective thermal conductivity decreases significantly downstream of the interface from upstream, then dissociative cooling may not be effective.

Acknowledgment

This work was supported by the U.S. Army Armament Research, Development, and Engineering Center under Contract DAAA21-93-C-0101.

References

[1]Lacy, B. P., Wilson, D. E., and Varghese, P. L., "Dissociative Cooling: Effect on Stagnation Heat Transfer of Gas Mixture Injection," *Journal of Spacecraft and Rockets*, Vol. 32, No. 5, 1995, pp. 777–782.

[2]Lacy, B., Wilson, D., and Varghese, P., "The Dissociative Cooling Concept, Part Two: The Effectiveness of Dissociation as Internal Cooling for a Porous Medium," AIAA Paper 94-1991, June 1994.

[3]Lide, D., *CRC Handbook of Chemistry and Physics*, 71st ed., CRC Press, Boca Raton, FL, 1990, p. 6-70.

[4]Mark, H. (ed.), *Kirk-Othmer Encyclopedia of Chemical Technology*, 3rd ed., Vol. 2, Wiley, New York, 1978, p. 521.

[5]Reshotko, E., and Cohen, C. B., "Heat Transfer at the Forward Stagnation Point of Blunt Bodies," NACA TN-3513, July 1955.

[6]Libby, P., "The Homogenous Boundary Layer at an Axisymmetric Stagnation Point with Large Rates of Injection," *Journal of the Aerospace Sciences*, Vol. 29, No. 1, 1962, pp. 48–60.

[7]Virnich, H., and Hopfner, A., "Der Isotopieeffekt bei der Verdampfung von Ammoniumchlorid," *Berichte der Bunsengesellschaft für Physikalrsche Chemie*, Vol. 84, No. 8, 1980, pp. 716–720.

[8]Scheidegger, A., *The Physics of Flow Through Porous Media*, 1st ed., Univ. of Toronto Press, Toronto, ON, Canada, 1958, p. 73.

[9]Eckert, E., and Drake, R., *Analysis of Heat and Mass Transfer*, 1st ed., McGraw–Hill, New York, 1972, pp. 142, 143.

[10]Nield, D., and Bejan, A., *Convection in Porous Media*, 1st ed., Springer–Verlag, New York, 1992, p. 237.

[11]Bejan, A., *Convection Heat Transfer*, 1st ed., Wiley, New York, 1984, p. 352.

[12]Bird, R., Stewart, W., and Lightfoot, E., *Transport Phenomena*, 1st ed., Wiley, New York, 1960, p. 570.

B. A. Bhutta
Associate Editor